



Contents lists available at ScienceDirect

Journal of Engineering Research

journal homepage: www.journals.elsevier.com/journal-of-engineering-research

Twisting morphing wings with tight geometric constraints for biomimetic swimming or flying robotic vehicles

Bing Luo^{a,b}, Weicheng Cui^b, Wei Li^{b,*}

^a School of Mechanical Engineering, Zhejiang University, Hangzhou, Zhejiang 310027, China

^b Key Laboratory of Coastal Environment and Resources of Zhejiang Province, School of Engineering, Westlake University, Hangzhou, Zhejiang 310030, China

ARTICLE INFO

Keywords:

Active twisting
Active torsion
Biomimetic robot
Morphing wing
Spanwise twisting
Twisting morphing wing

ABSTRACT

Active twisting morphing (ATM) wings have significant implications for biomimetic swimming or flying robotic vehicles. This article considers an ATM wing that has one shaft with many ribs, each rib is driven to swing in its individual plane that is perpendicular to the shaft, showing increasingly swing angles from the wing base to the wing-tip and thus form active wing twisting. For the overall twisting angle of the wing that is less than 90 degrees (e.g., during cruising operations of the robotic vehicles), we show that the geometry of mechanical implementations of the twisting wing can be further tightened using segment gears for transmission, instead of normal whole gears, which constraints have been largely unexplored. Here we provide the geometric constraints on the transmission with segment gears for such wing and give tighter feasible solutions of the constraints as well as provide the mechanical implementations using segment gears that are compact for ATM wings for biomimetic robotic vehicles.

Introduction

Morphing wings are commonly used for some aircraft, robotic birds, or robotic fish [1–8,10,12–18,23–30]. Wing twisting (or wing torsion [1]) of an active twisting morphing (ATM) wing is effective to control, e.g., flapping, roll, and yaw of a swimming or flying robot [1]. There are many methods to achieve twisting of morphing wings. Smartbird has active control of each wing twisting, which is achieved by a motor installed near the wing-tip, and the active wing twisting can improve aerodynamic efficiency more than 80 %, compared with passive wing twisting that is only about 30 % [1]. The outermost rib of each wing of SmartBird is installed on the motor, and as the motor rotates, this rib also rotates (swings) with respect to the spanwise axis of the wing. There are two elastic cables that connect the leading edges and the trailing edges of all the ribs, respectively, of each wing. Thus, the swinging of other ribs is driven by the outermost rib through the two elastic cables. That is, the wing twisting along the wing-span is largely induced by elastic materials, and the wing twisting cannot be fully controlled by the motor along, since the external aerodynamic or hydrodynamic loading on such wing also has significant influence on the wing twisting that is uncontrollable and also less easily measurable. There is few research on ATM wings with spanwise accurate twisting and large loading

transmissions to movable wing parts [2,13,34,35]. There are researches for passive twisting or deformation, e.g., the twisting wing with lattice-based cells [3], a morphing wing with a twisting tensegrity mechanism [4,31,32], the wings with aeroelastic structures [11], or with shape memory alloys [15,22,33].

Compared with Ref. [1], the mechanics of ATM wings are considered in Ref. [2]. For the simplest implementation of an ATM wing, there is a shaft driven by a motor that is installed at the wing base, a beam is fixed on the stator of the motor which is parallel to the shaft, and some ribs located on the shaft, each rib can swing in its individual plane that is perpendicular to the shaft, showing increasingly swing angles from the wing base to the wing-tip, as the shaft rotates, thus forming ATM wing that is similar to typical wing twisting of bird wings [16,18–20]. Usually, a wing can be covered with elastic materials as a skin to keep smooth between ribs for better aerodynamic or hydrodynamic performance [36, 37].

For given values of the center distance between the shaft and the beam and the radii of the cross-sections of the shaft and the beam, then, the ranges of the feasible radii of the gears (i.e., pitch circles, root circles, and outside circles), as well as the gear ratio, can be determined for the wing, but the range of the gear ratios is often limited and some gear ratios may be infeasible (typically lower than the feasible range) with

* Corresponding author.

E-mail address: wei.utdallas@live.com (W. Li).

<https://doi.org/10.1016/j.jer.2023.10.036>

Received 30 July 2023; Received in revised form 15 October 2023; Accepted 23 October 2023

Available online 27 October 2023

2307-1877/© 2023 The Authors. Published by Elsevier B.V. on behalf of Kuwait University. This is an open access article under the CC BY-NC-ND license (<http://creativecommons.org/licenses/by-nc-nd/4.0/>).

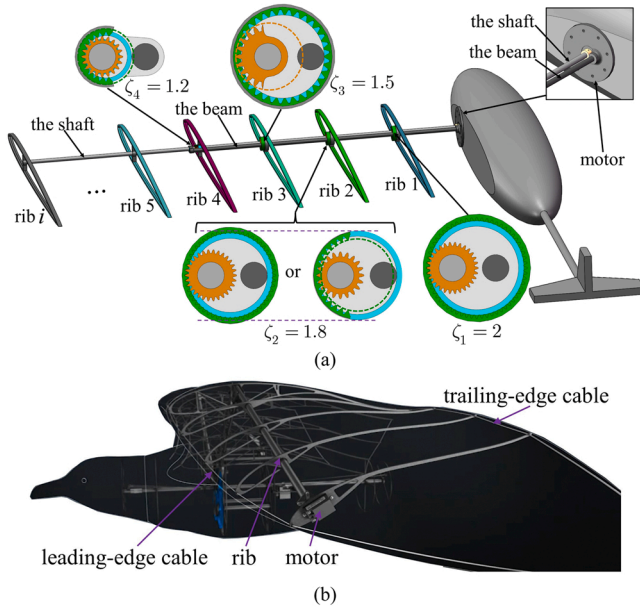


Fig. 1. (a) Illustration of a robotic wing with ATM capability. The gears for rib 1 are both whole gears. Gear B for rib 2 can be either a whole gear or a segment gear. While the gears for ribs 3 and 4 cannot be all whole gears. The wing flapping mechanism is omitted here as it is not the focus of this article. The skin of the wing is also omitted. (b) Active twisting (torsion) wing of SmartBird [1].

usual implementations for the geometric constraints. The feasible solutions of the constraints have been expanded in Ref. [2] by adjusting the center distance to be shorter of each pair of gears than the center distance between the shaft and the beam.

Usually, a cross-section of the wing is an airfoil, and its geometry is often a major concern for a better performance, and the tight height of the airfoil may be usually preferred, similar to the reduction of joint diameters [14]. For the overall twisting angle of the wing that is less than 90 degrees, typically for robots with only cruising operations [21], the geometry of implementations of wing twisting can be further tightened via gear transmission using segment gears, instead of using normal whole gears [2].

The main contributions of this article are as follows: Consider the typical swing angles of the ribs that are less than 90 degrees, for such scenarios, the transmission constraints are designed with segment gears, instead of using normal whole gears, for wing twisting, and then provide more tighter feasible solutions of the constraints, as well as mechanical implementations using segment gears that are compact for morphing wings of swimming or flying robots. The feasible solutions of the radii of the gears could be significantly extended compared with the results in Ref. [2] that are limited or even have no feasible solutions for whole gears.

The corresponding mechanical implementations have low control complexity, low inertia, and high robustness that can tolerate the deformations of the shaft and the beam; the properties of accurate active-twisting along the wing-span and large load transmissions to movable parts may be better than the material-elastic induced twisting along the wing-span of SmartBird [1]; and the motor installed at the wing base has less mass inertia and moment of inertia, compared with the case of the motor installed near the wing-tip for SmartBird [1]. Such a robotic twisting wing or twisting wing segments are applicable to the wings of, e.g., swimming or flying robotic vehicles [1,6,7,9,18–21].

The rest of this paper is arranged as follows: Section II is the description of the problem. Section III reviews the previous results. Section IV is the feasible solutions of the constraints with implementations for ATM wings. Section V is the conclusion. A video is also provided.

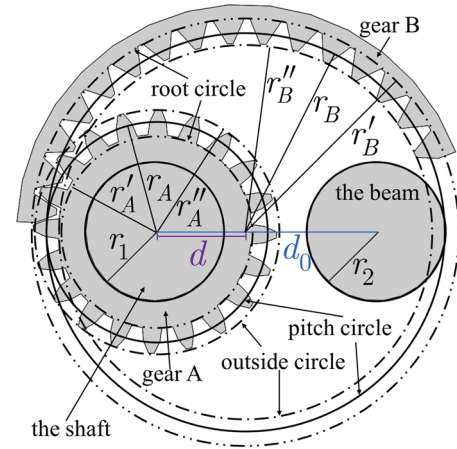


Fig. 2. Illustration of the meshing gears.

Problem description

This paper focuses on ATM of a robotic wing (Fig. 1). The shaft is driven by the rotor of the motor installed at the wing base, the beam fixed on the stator of the motor is parallel to the shaft; rib i swings with angle $\gamma_i \in \mathbb{R}$ in either the negative or positive direction in its swing plane, when the shaft rotates with rotation angle $\gamma_m \in \mathbb{R}$, $\gamma_m \in [-\gamma_0, \gamma_0]$, where $\gamma_0 > 0$ is the maximum wing twisting angle. Define $\delta_{r,i} := \gamma_i/\gamma_m \in (0, 1]$ as the twist-ratio of rib i , the positive direction represents the positive wing pitch. Consider gear transmission for the swing of a rib via a pair of gears, the external gear is fixed on the shaft, the internal gear is installed on the beam through a rolling bearing (the center of the rolling bearing does not necessarily be the center of the cross-sectional center of the beam) [2].

For the maximum wing twisting angle less than 90 degrees, i.e., $\gamma_0 < \pi/2$, then one or both gears for driving a rib can be made as segment gear(s), then, what are the feasible solutions?

For i th pair of gears for rib i , subscript i is used in notations. For clarity, we just consider two meshing gears and omit the subscript of notations. To achieve the twist-ratio of a rib, consider gear transmission by a pair of meshing gears, external gear A has radius $r_A > 0$ of the pitch circle, internal gear B has radius $r_B > 0$ of the pitch circle, the gear ratio, i.e., the inverse of the twist-ratio, is:

$$\zeta := r_B/r_A > 1, \quad (1)$$

For gear A, $r_A^- > r_A > r_A'$, where r_A' is the radius of the root circle, r_A^- is the radius of the outside circle. For gear B, $r_B^- > r_B > r_B'$, where r_B' is the radius of the root circle, r_B^- is the radius of the outside circle. Denote $\delta_A^- := r_A^- - r_A > 0$, $\delta_A' := r_A - r_A' > 0$, $\delta_B^- := r_B^- - r_B > 0$, $\delta_B' := r_B - r_B' > 0$. Usually, δ_A' , δ_A^- , δ_B' , and δ_B^- are very small, compared with the radii of the gears. The corresponding constraints are:

$$\delta_B^- > \delta_A^- > 0, \quad \delta_A' > \delta_B' > 0, \quad (2)$$

Remark 1. Inequalities (2) hold throughout this article and will not be repeated in each of the inequalities in the following of this article for the lack of space.

Denote $r_1 > 0$ and $r_2 > 0$ as the radii of the cross-section of the shaft and the beam, respectively. The distance between the cross-section centers of the shaft and the beam is $d_0 > 0$. r_1 , r_2 , and d_0 are constants that are predetermined,

$$d_0 > r_1 + r_2, \quad (3)$$

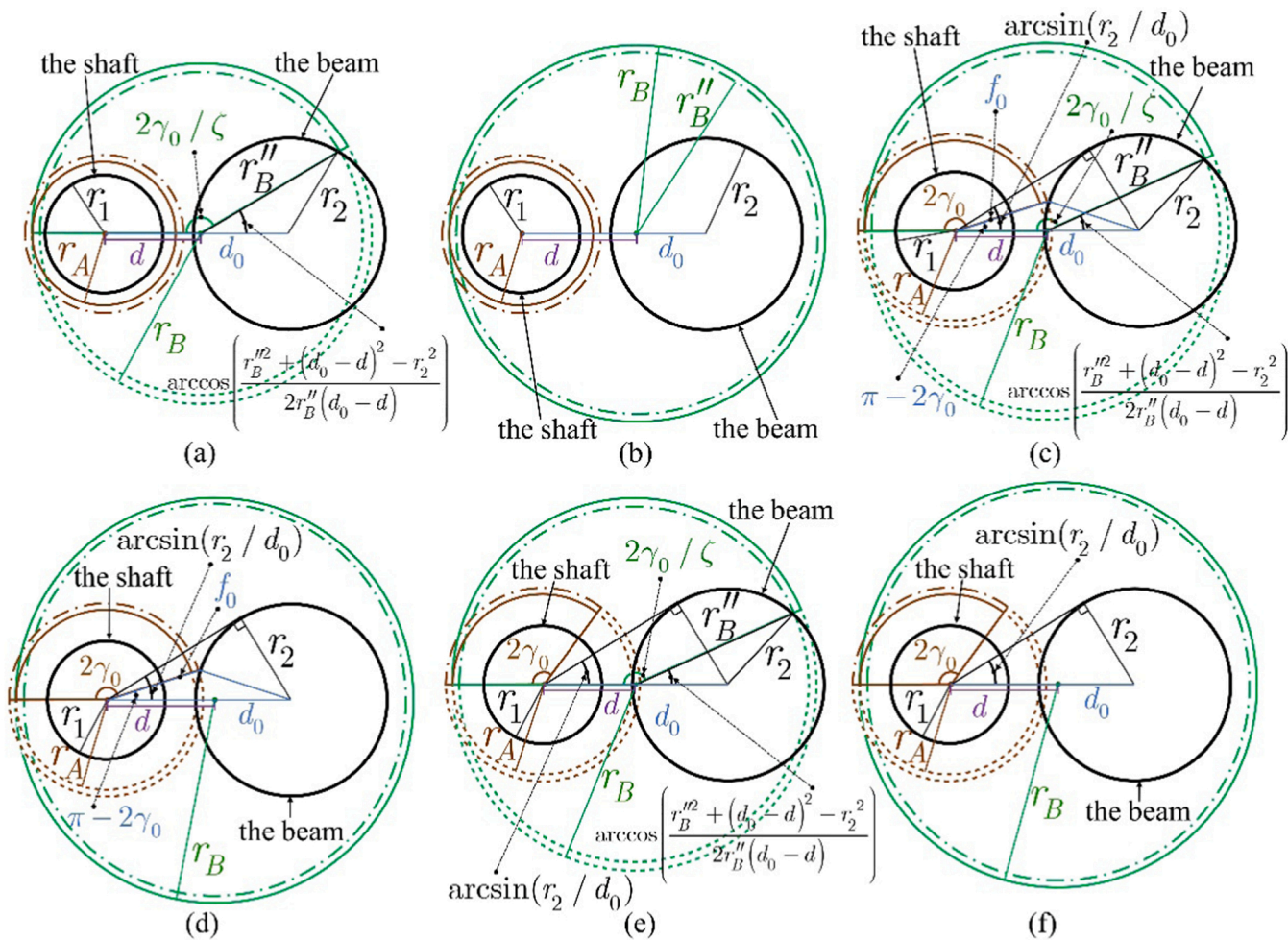


Fig. 3. Illustration of the meshing gears with $d \in [d_0 - r_2, d_0]$. (a) Gear A is a whole gear; gear B is a segment gear. (b) Gears A and B are whole gears. (c) Gears A and B are segment gears. (d) Gear A is a segment gear; gear B is a whole gear. (e) Gears A and B are segment gears. (f) Gear A is a segment gear; gear B is a whole gear.

Brief review of previous results

This section describes the previous results in Ref. [2] for self-containment of this article and for the comparative purpose.

The common implementation of gear transmission is that the centers of gears A and B are located at the cross-sectional centers of the shaft and the beam, respectively, thus, the center distance between the gears is:

$$r_B - r_A = d_0, \tag{4}$$

the geometric constraints for two meshing gears are:

$$\begin{cases} \zeta := r_B/r_A > 1, \\ r_B - r_A = d_0 > 0, \\ r_A \in (r_1 + \delta'_A, d_0 - r_2 - \delta'_A), \end{cases} \tag{5}$$

thus, in inequalities (5), the range of the gear ratio is:

$$\zeta \in \left(1 + \frac{d_0}{d_0 - r_2 - \delta'_A}, 1 + \frac{d_0}{r_1 + \delta'_A} \right), \tag{6}$$

and for r_A and r_B from Eqs. (1) and (4),

$$\begin{cases} r_A = r_A(\zeta) = \frac{d_0}{\zeta - 1}, \\ r_B = r_B(\zeta) = \frac{d_0 \zeta}{\zeta - 1}, \end{cases} \tag{7}$$

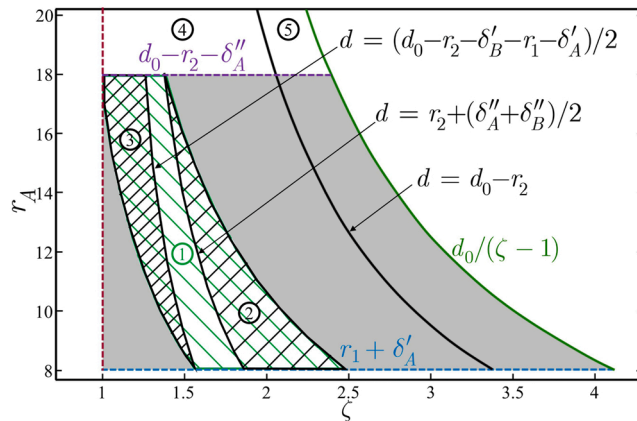


Fig. 5. Illustration of feasible solutions of r_A with respect to ζ . The gray areas represent the results in Fig. 6 of Ref. [2] also shown in Fig. A5. Area 1 is the result of Fig. 4(c), area 2 is the result of Fig. 4(a) and Fig. 3(a), area 3 is the result of Fig. 4(b), area 4 is the result of Fig. 4(d)–(f), and area 5 is the result of Fig. 3(c)–(f). Here the values of coordinates show the example with $d_0 = 25$, $r_1 = r_2 = 6$, $\delta'_A = \delta'_B = 2$, $\delta''_A = \delta''_B = 1$.

the feasible values of r_A , r_B , and ζ for inequalities (5) are in Fig. 3 of Ref. [2].

To solve the desired gear ratio that is lower than inequalities (6), one

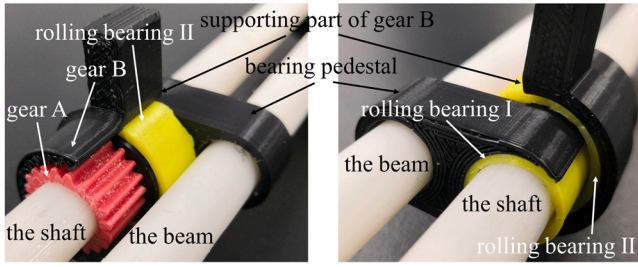


Fig. 6. An example from two perspectives. $\zeta = 1.2$, $d = 1.4$, $d_0 = 16$, $r_1 = r_2 = 5$, $\delta'_A = \delta'_B = 2$, $\delta''_A = \delta''_B = 1$, then $r_A = 7$, $r_B = 8.4$.

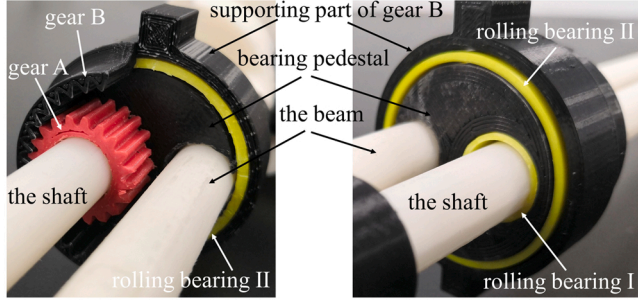


Fig. 7. An example from two perspectives. $\zeta = 1.8$, $d = 6.4$, $d_0 = 16$, $r_1 = r_2 = 5$, $\delta'_A = \delta'_B = 2$, $\delta''_A = \delta''_B = 1$, then $r_A = 8$, $r_B = 14.4$.

can adjust the center distance of the gears as:

$$d := r_B - r_A \in (0, d_0], \quad (8)$$

As a result, the center of gear B cannot coincide with the center of the cross-section of the beam. The center of gear A is located at the center of the cross-section of the shaft. From Eqs. (1) and (8),

$$\begin{cases} r_A = r_A(d, \zeta) = \frac{d}{\zeta - 1}, \\ r_B = r_B(d, \zeta) = \frac{d\zeta}{\zeta - 1}, \end{cases} \quad (9)$$

and the constraints are (Fig. 5 in Ref. [2]):

If the beam is in the envelop of gear B, then the constraints are:

$$\begin{cases} \zeta := r_B/r_A > 1, \\ d = r_B - r_A \in (0, d_0], \\ r_A \in (r_1 + \delta'_A, d_0 - r_2 - \delta'_A), \\ r_B > d_0 + r_2 + \delta'_B - d, \end{cases} \quad (10)$$

then, the ranges of d and ζ are:

$$\begin{aligned} d &\in \left(r_2 + \frac{\delta''_A + \delta''_B}{2}, d_0 \right], \\ \zeta &\in \left(1 + \frac{d}{d_0 - r_2 - \delta'_A}, 1 + \frac{d}{\max\{r_1 + \delta'_A, d_0 + r_2 + \delta'_B - 2d\}} \right), \end{aligned} \quad (11)$$

the range of inequalities (11) are generally lower than that of inequalities (6). Here inequalities (10) reduce to be inequalities (5) and inequalities (11) reduce to be inequalities (6), if $d = d_0$.

If the beam is out of the envelop of gear B, then:

$$\begin{cases} \zeta := r_B/r_A > 1, \\ d = r_B - r_A \in (0, d_0], \\ r_A \in (r_1 + \delta'_A, d_0 - r_2 - \delta'_A), \\ r_B < d_0 - r_2 - \delta'_B - d, \end{cases} \quad (12)$$

then:

$$\begin{aligned} d &\in \left(0, \frac{d_0 - r_2 - \delta'_B - r_1 - \delta'_A}{2} \right), \\ \zeta &\in \left(1 + \frac{d}{d_0 - r_2 - \delta'_B - 2d}, 1 + \frac{d}{r_1 + \delta'_A} \right). \end{aligned} \quad (13)$$

The values of ζ can be smaller than those of inequalities (11).

The feasible solutions of r_A and r_B with respect to ζ for inequalities (10) and (12) are provided in Fig. 6 of Ref. [2], which is also shown in Fig. A5 of the Appendix A.

Mechanical design for limited wing twisting

Consider gear A as a segment gear with angle $2\gamma_0$, then:

- 1) For $\gamma_0 \geq \pi/2$, the moving envelop of gear A is still the whole circle with radius r'_A .
- 2) For $\gamma_0 \in \left(\frac{\pi}{2} - \frac{1}{2} \arcsin\left(\frac{r_2}{d_0}\right), \frac{\pi}{2} \right)$, the moving envelop of gear A is not a whole circle and can relax the upper constraint of r_A , the geometric constraint of r_A with respect to the beam is that: $r_A + \delta'_A < f_0$, where the function $f_0 = f_0(d_0, \gamma_0)$ is computed from the law of cosines that relates the lengths of the sides of a triangle to the cosine of one of its angles, as illustrated in Fig. 3(c) and (d): $r_2^2 = f_0^2 + d_0^2 - 2f_0d_0\cos(\pi - 2\gamma_0)$, i.e.,

$$f_0 = -d_0\cos(2\gamma_0) - \sqrt{d_0^2\cos^2(2\gamma_0) - (d_0^2 - r_2^2)} > d_0 - r_2 > 0, \quad (14)$$
 also, since $d_0 > r_2$, then, $\arcsin(r_2/d_0) \in (0, \pi/2)$, thus, $2\gamma_0 \in (\pi/2, \pi)$, so $\cos(2\gamma_0) < 0$, that is, $f_0 > 0$.
- 3) For $\gamma_0 < \frac{\pi}{2} - \frac{1}{2} \arcsin\left(\frac{r_2}{d_0}\right)$, there is no constraint for gear A with respect to the beam.

The center of gear B in the radius of the beam

Here the center distance of the gears as $d \in [d_0 - r_2, d_0]$ is considered. Then:

- 1) For $\gamma_0 \geq \pi/2$, the constraints are:

$$\begin{cases} \zeta := r_B/r_A > 1, \\ d = r_B - r_A \in [d_0 - r_2, d_0], \\ \gamma_0 \geq \pi/2, \\ \frac{\gamma_0}{\zeta} \leq \frac{\pi}{2} - \frac{1}{2} \arccos\left(\frac{r_B^2 + (d_0 - d)^2 - r_2^2}{2r'_B(d_0 - d)}\right), \\ r_B \leq \delta'_B + d_0 + r_2 - d, \\ r_A \in (r_1 + \delta'_A, d_0 - r_2 - \delta'_A), \end{cases} \quad (15)$$

as illustrated in Fig. 3(a), or

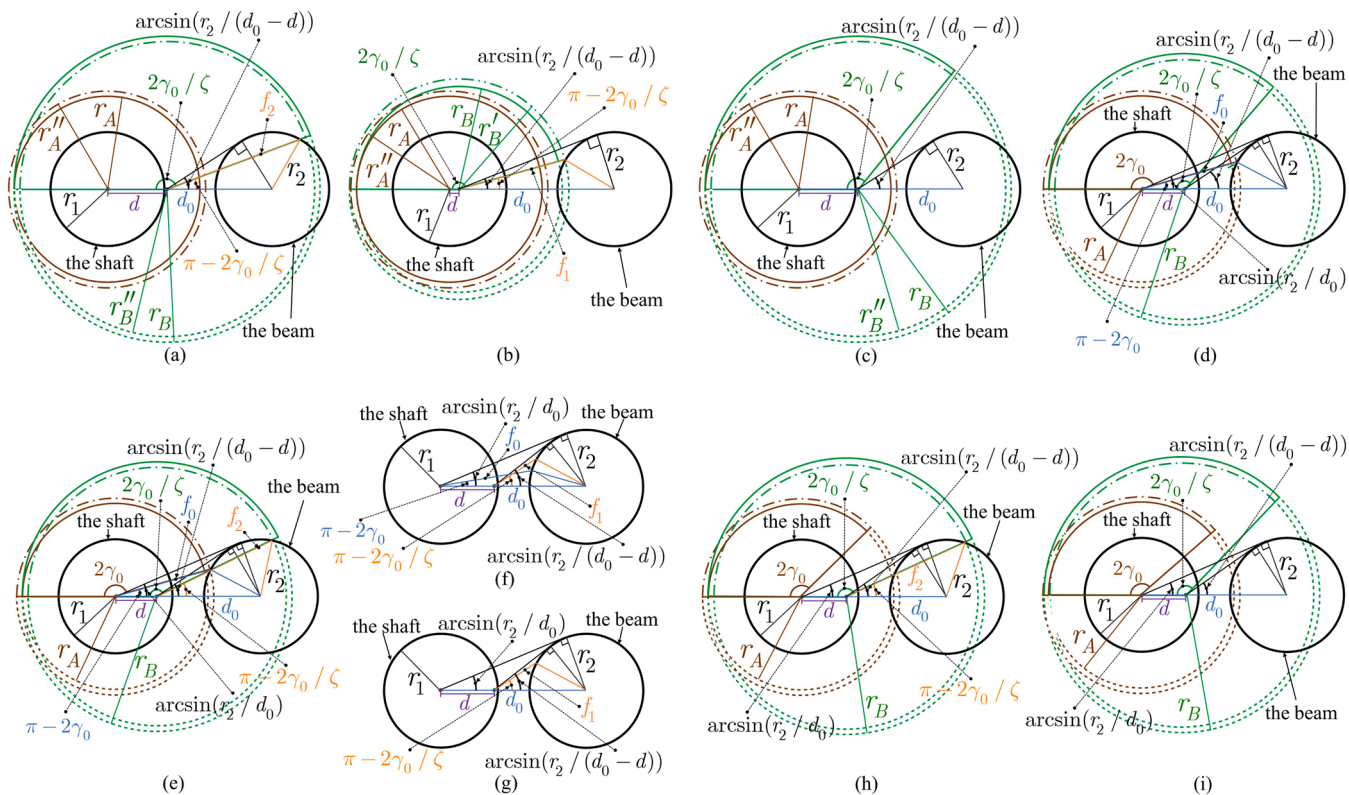


Fig. 4. Illustration of the meshing gears with $d \in (0, d_0 - r_2)$. (a)–(c) Gear A is a whole gear; gear B is a segment gear. (d)–(i) Gears A and B are segment gears.

$$\left\{ \begin{array}{l} \zeta := r_B/r_A > 1, \\ d = r_B - r_A \in [d_0 - r_2, d_0], \\ \gamma_0 \geq \pi/2, \\ r_B > \delta_B^{\ddot{}} + d_0 + r_2 - d, \\ r_A \in (r_1 + \delta_A^{\ddot{}}, d_0 - r_2 - \delta_A^{\ddot{}}), \end{array} \right. \quad (16)$$

as illustrated in Fig. 3(b).

2) For $\gamma_0 \in (\frac{\pi}{2} - \frac{1}{2} \arcsin(\frac{r_2}{d_0}), \frac{\pi}{2})$, the constraints are that:

$$\left\{ \begin{array}{l} \zeta := r_B/r_A > 1, \\ d = r_B - r_A \in [d_0 - r_2, d_0], \\ \gamma_0 \in (\frac{\pi}{2} - \frac{1}{2} \arcsin(\frac{r_2}{d_0}), \frac{\pi}{2}), \\ \frac{\gamma_0}{\zeta} \leq \frac{\pi}{2} - \frac{1}{2} \arccos\left(\frac{r_B^2 + (d_0 - d)^2 - r_2^2}{2r_B(d_0 - d)}\right), \\ r_B \leq \delta_B^{\ddot{}} + d_0 + r_2 - d, \\ r_A \in (d_0 - r_2 - \delta_A^{\ddot{}}, f_0 - \delta_A^{\ddot{}}), \end{array} \right. \quad (17)$$

as illustrated in Fig. 3(c), or

$$\left\{ \begin{array}{l} \zeta := r_B/r_A > 1, \\ d = r_B - r_A \in [d_0 - r_2, d_0], \\ \gamma_0 \in (\frac{\pi}{2} - \frac{1}{2} \arcsin(\frac{r_2}{d_0}), \frac{\pi}{2}), \\ r_B > \delta_B^{\ddot{}} + d_0 + r_2 - d, \\ r_A \in (d_0 - r_2 - \delta_A^{\ddot{}}, f_0 - \delta_A^{\ddot{}}), \end{array} \right. \quad (18)$$

as in Fig. 3(d); the upper constraint $r_A + \delta_A^{\ddot{}} < d_0 - r_2$ in inequalities (5) is relaxed by $r_A + \delta_A^{\ddot{}} < f_0$, since $f_0 > d_0 - r_2$. Here the lower

bound of ζ can be smaller, compared with inequalities (5).

3) For $\gamma_0 < \frac{\pi}{2} - \frac{1}{2} \arcsin(\frac{r_2}{d_0})$, the constraints are that:

as illustrated in Fig. 3(e), or

$$\left\{ \begin{array}{l} \zeta := r_B/r_A > 1, \\ d = r_B - r_A \in [d_0 - r_2, d_0], \\ \gamma_0 \in (0, \frac{\pi}{2} - \frac{1}{2} \arcsin(\frac{r_2}{d_0})), \\ r_B > \delta_B^{\ddot{}} + d_0 + r_2 - d, \\ r_A > d_0 - r_2 - \delta_A^{\ddot{}}, \end{array} \right. \quad (19)$$

as illustrated in Fig. 3(f).

The center of gear B outside the radius of the beam

Here gear B is also considered as a segment gear, with angle $2\gamma_0/\zeta$, which is less than $2\gamma_0$, then:

- 1) If $\gamma_0 \geq \pi\zeta/2$, then the envelopes of the motions of gears A and B are whole circles.
- 2) If $\frac{f_0}{\zeta} \in (\frac{\pi}{2} - \frac{1}{2} \arcsin(\frac{r_2}{d_0 - d}), \frac{\pi}{2})$, where $d_0 - d > r_2$, then the geometric constraint of r_B with respect to the beam is that: $r_B < f_1 - \delta_B^{\ddot{}}$, or $r_B > f_2 + \delta_B^{\ddot{}}$, where:

$$\begin{aligned} f_1 &= -\left(d_0 - d\right) \cos\left(\frac{2\gamma_0}{\zeta}\right) - \sqrt{\left(d_0 - d\right)^2 \cos^2\left(\frac{2\gamma_0}{\zeta}\right) - \left(d_0 - d\right)^2 + r_2^2} \\ &> d_0 - d - r_2 > 0, \end{aligned} \quad (20)$$

$$f_2 = -\left(d_0 - d\right) \cos\left(\frac{2\gamma_0}{\zeta}\right) + \sqrt{\left(d_0 - d\right)^2 \cos^2\left(\frac{2\gamma_0}{\zeta}\right) - \left(d_0 - d\right)^2 + r_2^2} > f_1, \quad (21)$$

refer to Fig. 4(a) and (b); since $d_0 - d > r_2$, then,

$$\arcsin\left(\frac{r_2}{d_0 - d}\right) \in \left(0, \frac{\pi}{2}\right),$$

thus, $2\gamma_0/\zeta \in (\pi/2, \pi)$, so $\cos(2\gamma_0/\zeta) < 0$, that is, $f_1 > 0, f_2 > 0$, and

$$\frac{\pi}{2} - \frac{1}{2} \arcsin\left(\frac{r_2}{d_0 - d}\right) \in \left(\frac{\pi}{4}, \frac{\pi}{2}\right). \quad (22)$$

3) If $\frac{\gamma_0}{\zeta} \leq \frac{\pi}{2} - \frac{1}{2} \arcsin\left(\frac{r_2}{d_0 - d}\right)$, where $d_0 - d > r_2$, then gear B has no conflict with the beam, as in Fig. 4(i):

For some values of γ_0, ζ , and $d \in (0, d_0 - r_2)$, the constraints are:

- 1) If $\gamma_0 \geq \pi\zeta/2$, the results are same as inequalities (10)-(13).
- 2) If $\gamma_0 \in [\pi/2, \pi\zeta/2)$, then only the envelop of the motion of gear A is a whole circle, in this case,

• if

$\frac{\gamma_0}{\zeta} \in \left(\frac{\pi}{2} - \frac{1}{2} \arcsin\left(\frac{r_2}{d_0 - d}\right), \frac{\pi}{2}\right)$, where $d_0 - d > r_2$, then the geometric constraints are that:

$$\begin{cases} \zeta := r_B/r_A > 1, \\ d = r_B - r_A \in (0, d_0 - r_2), \\ \gamma_0 \in [\pi/2, \pi\zeta/2), \\ \frac{\gamma_0}{\zeta} \in \left(\frac{\pi}{2} - \frac{1}{2} \arcsin\left(\frac{r_2}{d_0 - d}\right), \frac{\pi}{2}\right), \\ r_A \in (r_1 + \delta'_A, d_0 - r_2 - \delta'_A), \\ r_B < f_1 - \delta'_B, \text{ or } r_B > f_2 + \delta'_B, \end{cases} \quad (23)$$

as illustrated in Fig. 4(a) and (b),

• if

$\frac{\gamma_0}{\zeta} \leq \frac{\pi}{2} - \frac{1}{2} \arcsin\left(\frac{r_2}{d_0 - d}\right)$, where $d_0 - d > r_2$, then:

$$\begin{cases} \zeta := r_B/r_A > 1, \\ d = r_B - r_A \in (0, d_0 - r_2), \\ \frac{\gamma_0}{\zeta} \leq \frac{\pi}{2} - \frac{1}{2} \arcsin\left(\frac{r_2}{d_0 - d}\right), \\ \gamma_0 \in [\pi/2, \pi\zeta/2), \\ r_A \in (r_1 + \delta'_A, d_0 - r_2 - \delta'_A), \end{cases} \quad (24)$$

as illustrated in Fig. 4(c).

- 3) For $\gamma_0 \in \left(\frac{\pi}{2} - \frac{1}{2} \arcsin\left(\frac{r_2}{d_0}\right), \frac{\pi}{2}\right)$, and in this case,

• if

$\frac{\gamma_0}{\zeta} \in \left(\frac{\pi}{2} - \frac{1}{2} \arcsin\left(\frac{r_2}{d_0}\right), \frac{\pi}{2}\right)$, where $d_0 - d > r_2$, then:

$$\begin{cases} \zeta := r_B/r_A > 1, \\ d = r_B - r_A \in (0, d_0 - r_2), \\ \gamma_0 \in \left(\frac{\pi}{2} - \frac{1}{2} \arcsin\left(\frac{r_2}{d_0}\right), \frac{\pi}{2}\right), \\ \frac{\gamma_0}{\zeta} \in \left(\frac{\pi}{2} - \frac{1}{2} \arcsin\left(\frac{r_2}{d_0 - d}\right), \frac{\pi}{2}\right), \\ r_A \in (d_0 - r_2 - \delta'_A, f_0 - \delta'_A), \\ r_B < f_1 - \delta'_B, \text{ or } r_B > f_2 + \delta'_B, \end{cases} \quad (25)$$

as illustrated in Fig. 4(e) and (f),

• if

$\frac{\gamma_0}{\zeta} \leq \frac{\pi}{2} - \frac{1}{2} \arcsin\left(\frac{r_2}{d_0 - d}\right)$, where $d_0 - d > r_2$, then:

$$\begin{cases} \zeta := r_B/r_A > 1, \\ d = r_B - r_A \in (0, d_0 - r_2), \\ \gamma_0 \in \left(\frac{\pi}{2} - \frac{1}{2} \arcsin\left(\frac{r_2}{d_0}\right), \frac{\pi}{2}\right), \\ \frac{\gamma_0}{\zeta} \leq \frac{\pi}{2} - \frac{1}{2} \arcsin\left(\frac{r_2}{d_0 - d}\right), \\ r_A \in (d_0 - r_2 - \delta'_A, f_0 - \delta'_A). \end{cases} \quad (26)$$

as illustrated in Fig. 4(d).

- 4) If $\gamma_0 < \frac{\pi}{2} - \frac{1}{2} \arcsin\left(\frac{r_2}{d_0}\right)$, and in this case,

• if

$\frac{\gamma_0}{\zeta} \geq \frac{\pi}{2} - \frac{1}{2} \arcsin\left(\frac{r_2}{d_0 - d}\right)$, where $d_0 - d > r_2$, then:

$$\begin{cases} \zeta := r_B/r_A > 1, \\ d = r_B - r_A \in (0, d_0 - r_2), \\ \gamma_0 \in \left[\frac{\pi\zeta}{2} - \frac{\zeta}{2} \arcsin\left(\frac{r_2}{d_0 - d}\right), \frac{\pi}{2} - \frac{1}{2} \arcsin\left(\frac{r_2}{d_0}\right)\right), \\ r_A > d_0 - r_2 - \delta'_A, \\ r_B < f_1 - \delta'_B, \text{ or } r_B > f_2 + \delta'_B, \end{cases} \quad (27)$$

as illustrated in Fig. 4(g) and (h),

• if $\frac{\gamma_0}{\zeta} < \frac{\pi}{2} - \frac{1}{2} \arcsin\left(\frac{r_2}{d_0 - d}\right)$, where $d_0 - d > r_2$, then:

$$\begin{cases} \zeta := r_B/r_A > 1, \\ d = r_B - r_A \in (0, d_0 - r_2), \\ \gamma_0 < \min\left\{\frac{\pi}{2} - \frac{1}{2} \arcsin\left(\frac{r_2}{d_0}\right), \frac{\pi\zeta}{2} - \frac{\zeta}{2} \arcsin\left(\frac{r_2}{d_0 - d}\right)\right\}, \\ r_A > d_0 - r_2 - \delta'_A, \end{cases} \quad (28)$$

as illustrated in Fig. 4(i).

Compared with inequalities (12) and (13), the constraints in inequalities (12):

$r_A < d_0 - r_2 - \delta'_A$ and $r_B < d_0 - r_2 - \delta'_B - d$ are relaxed in inequalities (28), which constraints are infeasible for implementations with normal whole gears.

Results and implementations

The feasible solutions of gear A are illustrated in Fig. 5, whereas the solutions of gear B can be obtained via Eq. (1), so we omit them here. In Fig. 5, the solution regions of r_A are extended by using segment gears compared with previous results shown in Fig. A5. Making gear A as a whole gear while keeping gear B as a segment gear has the following merits: 1) more tighter design of gears A and B in area 2, i.e., relaxation of the lower constraint of gear A in larger gear ratios that are usually used in the proximal part of the wing; 2) relaxation of the upper constraint of gear A in smaller gear ratios that are usually used in the distal part of the wing; 3) area 1 not only relaxes the lower and the upper constraints of gear A but also fills the gap region caused by the pre-determined values of r_1, r_2, d_0 , and γ_0 . For gear A as a segment gear, the sizes of gears A and B are larger, then can be used to against larger external loads especially for smaller gear ratios.

Therefore, the design of gears A and B is comprehensive within tight geometry constrains via adjusting ζ, d and γ_0 .

Here two implementations with segment gears are shown in Figs. 6 and 7. In Fig. 6, this implementation is in area 3 of Fig. 5 with respect to Fig. 4(b), with the predetermined parameters, there is no feasible

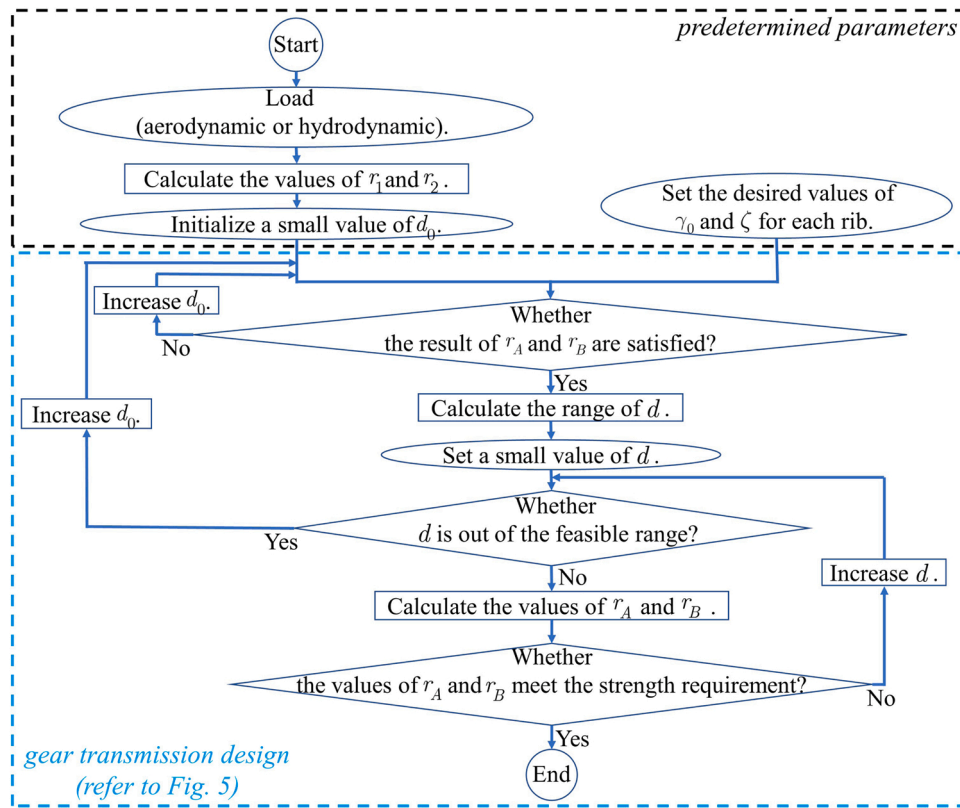


Fig. 8. An Illustration of the design flow chart for the gear transmission.

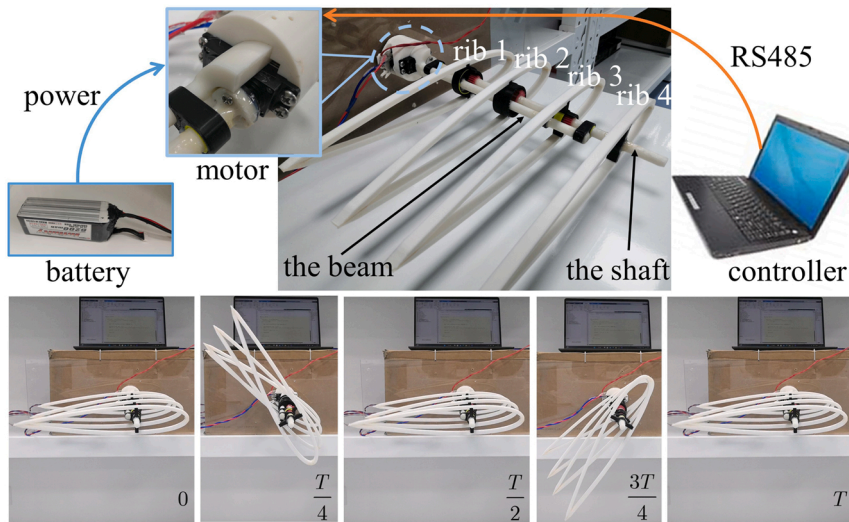


Fig. 9. Physical implementation of a morphing wing with tight geometric constraints and its morphing.

solutions for whole gears A and B, only segment gear transmission is available. In Fig. 7, this implementation is in area 2 of Fig. 5 with respect to Fig. 4(a), with the predetermined parameters, the feasible solutions of gears A and B can be tightened with the segment gear transmission compared with the whole gear transmission.

A flow chart is provided for ATM wings shown in Fig. 8. It provides the procedures to design ATM wings including the “predetermined parameters” part and the “gear transmission design” part, in which the “predetermined parameters” part is not the focus of this paper and thus omitted. The “gear transmission design” part is an iterative procedure of ATM wings design.

Finally, a physical implementation of a morphing wing with tight geometric constraints is provided in Fig. 9. The gear ratios of ribs 1–4 are 1.8, 1.5, 1.2, and 1, respectively. A kinematic experiment is shown in Fig. 9 and the supplementary video. The wing shows gradual twisting from the wing base to the wing-tip with respect to the motor. The wing can also be covered with elastic materials as a skin, which is not the focus of this paper and thus omitted.

Conclusion

This article considers design for an active twisting wing. For the

twisting angle less than 90 degrees, the implementations can be further tightened via gear transmission using segment gears, instead of normal whole gears. We provide more tighter feasible solutions of the constraints as well as implementations that are compact for morphing wings of swimming or flying robots.

There are some future considerations, for example, the skin design with elastic materials, external hydrodynamic or aerodynamic experiments with active wing morphing control, an automatic optimal design software for gear transmission design of each rib of ATM wing, etc.

Declaration of Competing Interest

The authors declare that they have no conflict of interest that could have appeared to influence the work reported in this paper.

Acknowledgments

This work was funded by the National Key Research and Development Program of China (2022YFC2805200) and the Startup funding of New-joined PI of Westlake University (041030150118).

Appendix A

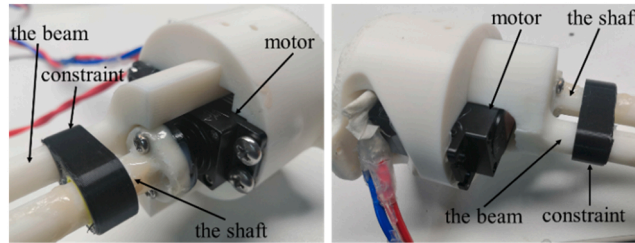


Fig. A1. . Illustration of the connection between the shaft, the beam, and motor.

For the physical implementation, the motor is fixed on the fuselage, the beam is fixed on the stator of the motor, the shaft is connected with the rotor of the motor, the constraint is aim to augment the stiffness of the wing during the wing locomotion.

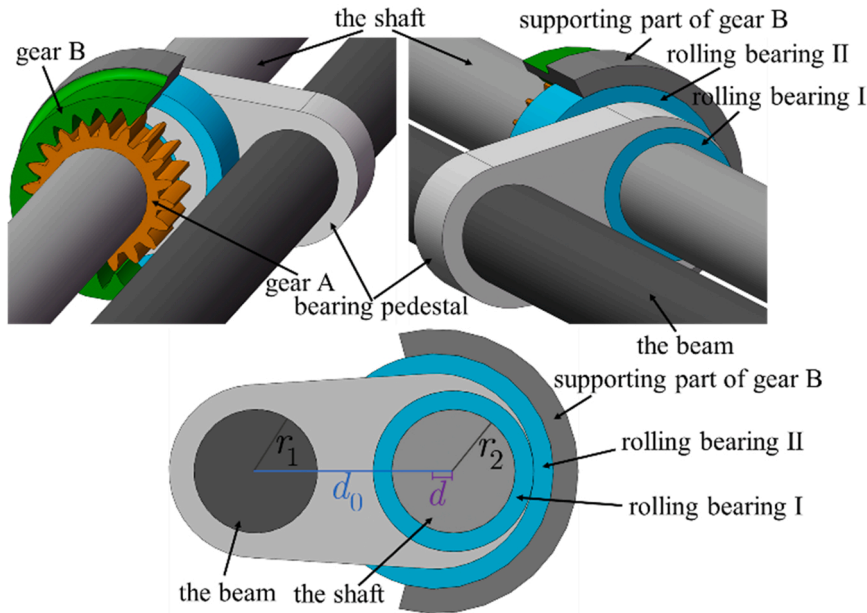


Fig. A2. . An example of CAD design refers to Fig. 6. $\zeta = 1.2$, $d = 1.4$, $d_0 = 16$, $r_1 = r_2 = 5$, $\delta'_A = \delta'_B = 2$, $\delta''_A = \delta''_B = 1$, then $r_A = 7$, $r_B = 8.4$.

The CAD model of the implementation in Fig. 6 for the segment gear transmission is in area 3 of Fig. 5 with respect to Fig. 4(b).

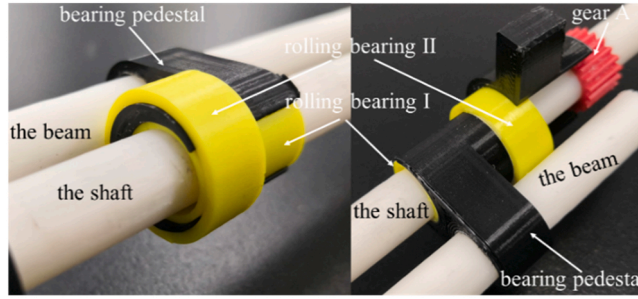


Fig. A3. . The exploded view of the design of Fig. 6.

The assemble detail of the implementation in Fig. 6 is shown in Fig. A3 with the exploded view.

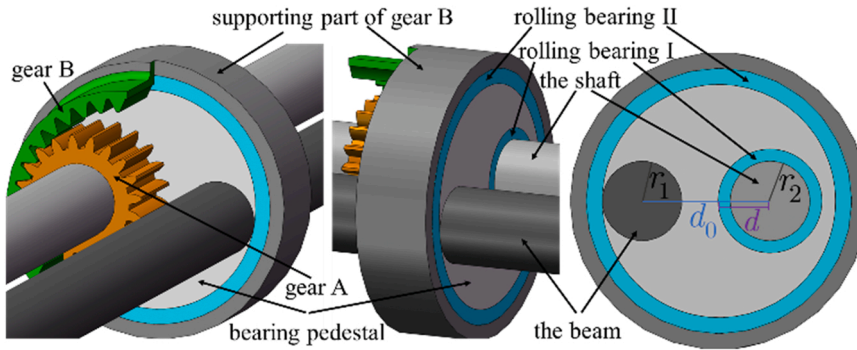


Fig. A4. . An example of CAD design refers to Fig. 7. $\zeta = 1.8$, $d = 6.4$, $d_0 = 16$, $r_1 = r_2 = 5$, $\delta'_A = \delta'_B = 2$, $\delta''_A = \delta''_B = 1$, then $r_A = 8$, $r_B = 14.4$.

The CAD model of the implementation in Fig. 7 for the segment gear transmission is in area 2 of Fig. 5 with respect to Fig. 4(a).

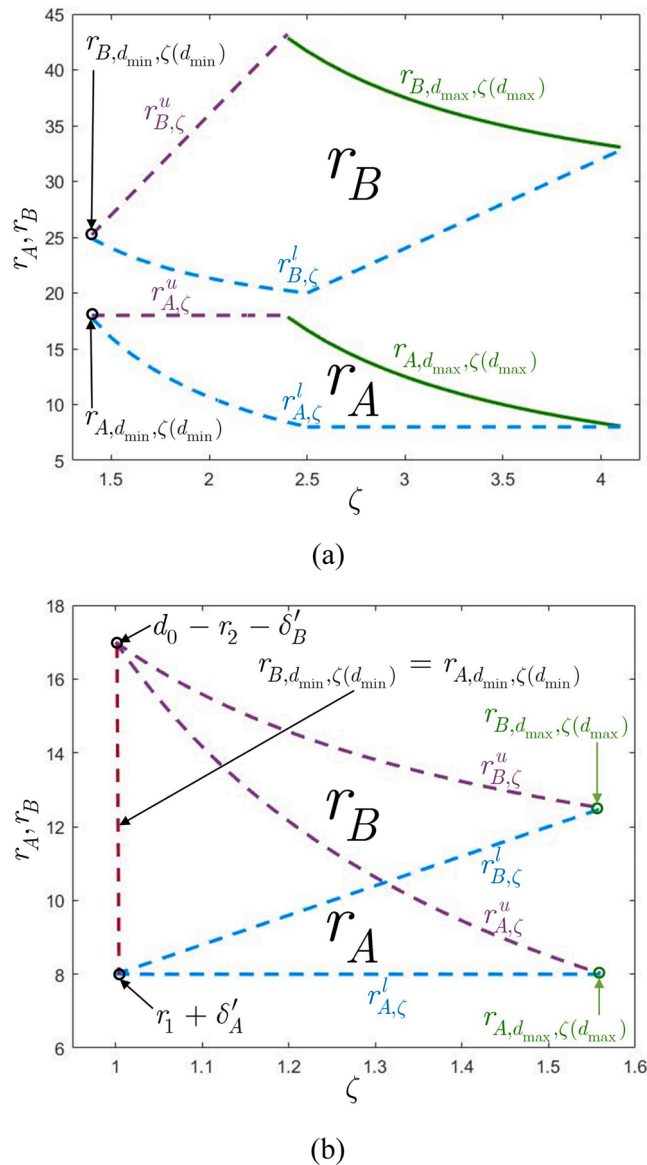


Fig. A5. Illustration of the feasible solutions (regions) of r_A and r_B with respect to ζ . Here the values of coordinates show the example with $d_0 = 25$, $r_1 = r_2 = 6$, $\delta'_A = \delta'_B = 2$, $\delta_A = \delta_B = 1$. (a) The feasible regions for inequalities (10). (b) The feasible regions for inequalities (12).

The solution regions of the whole gear transmission from Ref. [2] are shown in Fig. A5

References

- [1] D. Mackenzie, A flapping of wings, *Science* 335 (2012) 1430–1433.
- [2] B. Luo, W. Cui, W. Li, Active and robust twisting morphing wings with geometric constraints for flying or swimming robots, *IEEE/ASME Trans. Mechatron.* 27 (2022) 4205–4210.
- [3] B. Jenett, S. Calisch, D. Cellucci, N. Cramer, N. Gershenfeld, S. Swei, K.C. Cheung, Digital morphing wing: active wing shaping concept using composite lattice-based cellular structures, *Soft Robot.* 4 (2017) 33–48.
- [4] N.K. Pham, E.A.P. Hernandez, Modeling and design exploration of a morphing wing enabled by a twisting tensegrity soluti, *AIAA Scitech Forum* (2021), 2021–0099.
- [5] M. Di Luca, S. Mintchev, G. Heitz, F. Noca, D. Floreano, Bioinspired morphing wings for extended flight envelope and roll control of small drones, *Interface Focus* 7 (2017) 20160092.
- [6] J.S. Izraelevitz, M.S. Triantafyllou, A novel degree of freedom in flapping wings shows promise for a dual aerial/aquatic vehicle propulsor, in: *Proceedings of the 2015 IEEE International Conference on Robotics and Automation*. IEEE, 2015, p. 5830–5837.
- [7] H. Rodrigue, S. Cho, M.W. Han, B. Bhandari, J.E. Shim, S.H. Ahn, Effect of twist morphing wing segment on aerodynamic performance of UAV, *J. Mech. Sci. Technol.* 30 (2016) 229–236.
- [8] B.A. Rocca, S. Preidikman, M.L. Verstraete, D.T. Mook, Influence of spanwise twisting and bending on lift generation in MAV-like flapping wings, *J. Aerosp. Eng.* 30 (1) (2017).
- [9] S.A. Fazelzadeh, M. Rezaei, A. Mazidi, Aeroelastic analysis of swept pre-twisted wings, *J. Fluids Struct.* 95 (2020), 103001.
- [10] H.V. Phan, Q.T. Truong, H.C. Park, An experimental comparative study of the efficiency of twisted and flat flapping wings during hovering flight, *Bioinspir. Biomim.* 12 (2017), 036009.
- [11] N.B. Cramer, D.W. Cellucci, O.B. Formoso, C.E. Gregg, B.E. Jenett, J.H. Kim, M. Lendraitis, S.S. Swei, G.T. Trinh, K.V. Trinh, K.C. Cheung, Elastic shape morphing of ultralight structures by programmable assembly, *Smart Mater. Struct.* 28 (2019), 055006.
- [12] R.M. Ajaj, M.I. Friswell, W.G. Dettmer, G. Allegri, A.T. Isikveren, Dynamic modelling and actuation of the adaptive torsion wing, *J. Intell. Mater. Syst. Struct.* 24 (2013) 2045–2057.
- [13] S. Ameduri, A. Concilio, Morphing wings review: aims, challenges, and current open issues of a technology, *Proc. IMechE Part C* (2020).
- [14] S.R. Hummel, C. Chassapis, Configuration design and optimization of universal joints with manufacturing tolerances, *Mech. Mach. Theory* 35 (2000) 463–476.

- [15] S. Ameduri, A. Brindisi, B. Tiseo, A. Concilio, R. Pecora, Optimization and integration of shape memory alloy (SMA)-based elastic actuators within a morphing flap architecture, *J. Intell. Mater. Syst. Struct.* 23 (4) (2012) 381–396.
- [16] M. Maeda, T. Nakata, I. Kitamura, H. Tanaka, H. Liu, Quantifying the dynamic wing morphing of hovering hummingbird, *R. Soc. Open Sci.* 4 (2017), 170307.
- [17] G. Jodin, Y.B. Tekap, J.M. Saucray, J.F. Rouchon, M. Triantafyllou, M. Braza, Optimized design of real-scale A320 morphing high-lift flap with shape memory alloys and innovative skin, *Smart Mater. Struct.* 27 (2018), 115005.
- [18] M. Fluck, C. Crawford, A lifting line model to investigate the influence of tip feathers on wing performance, *Bioinspir Biomim.* 9 (2014), 046017.
- [19] G. Iosilevskii, Forward flight of birds revisited. Part 1: aerodynamics and performance, *R. Soc. Open Sci.* 1 (2014), 140248.
- [20] P. Henningsson, A. Hedenstrom, R.J. Bomphrey, Efficiency of lift production in flapping and gliding flight of swifts, *PLoS One* 9 (2) (2014), e90170.
- [21] Y. Shen, N. Harada, S. Katagiri, H. Tanaka, Biomimetic realization of a robotic penguin wing: Design and thrust characteristics, *IEEE/ASME Trans. Mechatron.* 26 (2021) 2350–2361.
- [22] H. Basaeri, A. Yousefi-Koma, M.R. Zakerzadeh, S.S. Mohtasebi, Experimental study of a bio-inspired robotic morphing wing mechanism actuated by shape memory alloy wires, *Mechatronics* 24 (2014) 1231–1241.
- [23] J. Wang, Y. Zhao, F. Xi, Y. Tian, Design and analysis of a configuration-based lengthwise morphing structure, *Mech. Mach. Theory* 147 (2020), 103767.
- [24] A. Moosavian, F. Xi, Modular design of parallel robots with static redundancy, *Mech. Mach. Theory* 96 (2016) 26–37.
- [25] Y. Zhao, F. Xi, Y. Tian, W. Wang, L. Li, Design of a planar hyper-redundant lockable mechanism for shape morphing using a centralized actuation method, *Mech. Mach. Theory* 165 (2021), 104439.
- [26] T. Ozaki, K. Hamaguchi, Improved lift force of a resonant-driven flapping-wing micro aerial vehicle by suppressing wing–body and wing–wing vibration coupling, *Extrem. Mech. Lett.* 40 (2020), 100867.
- [27] S. Yin, Z. Jia, X. Li, J. Zhu, Y. Xu, T. Li, Machine-learning-accelerated design of functional structural components in deep-sea soft robots, *Extrem. Mech. Lett.* 52 (2022), 101635.
- [28] D.M. Boston, F.R. Phillips, T.C. Henry, A.F. Arrieta, Spanwise wing morphing using multistable cellular metastructures, *Extrem. Mech. Lett.* 53 (2022), 101706.
- [29] K. Yokota, F. Barthelat, Stiff bioinspired architected beams bend Saint-Venant's principle and generate large shape morphing, *Int. J. Solids Struct.* 274 (2023), 112270.
- [30] D. Kumar, S.F. Ali, A. Arockiarajan, Theoretical and experimental studies on large deflection analysis of double corrugated cantilever structures, *Int. J. Solids Struct.* 228 (2021), 111126.
- [31] K.W. Moored, H. Bart-Smith, Investigation of clustered actuation in tensegrity structures, *Int. J. Solids Struct.* 46 (2009) 3272–3281.
- [32] K.W. Moored, T.H. Kemp, N.E. Houle, H. Bart-Smith, Analytical predictions, optimization, and design of a tensegrity-based artificial pectoral fin, *Int. J. Solids Struct.* 48 (2011) 3142–3159.
- [33] D.M. Elzey, A.Y.N. Sofla, H.N.G. Wadley, A shape memory-based multifunctional structural actuator panel, *Int. J. Solids Struct.* 42 (2005) 1943–1955.
- [34] A. Schlup, P. Bishay, T. McLennan, C. Barajas, B. Talebian, G. Thatcher, R. Flores, J. Perez-Norwood, C. Torres, K. Kibret, E. Guzman, MataMorph 2: A new experimental UAV with twist-morphing wings and camber-morphing tail stabilizers, in: *AIAA Scitech 2021 Forum*. Presented at the AIAA Scitech 2021 Forum, American Institute of Aeronautics and Astronautics, VIRTUAL EVENT.
- [35] H. Rodrigue, S. Cho, M.W. Han, B. Bhandari, J.E. Shim, S.H. Ahn, Effect of twist morphing wing segment on aerodynamic performance of UAV, *J. Mech. Sci. Technol.* 30 (2016) 229–236.
- [36] D. Ahmad, R.M. Ajaj, Multiaxial mechanical characterization of latex skin for morphing wing application, *Polym. Test.* 106 (2022), 107408.
- [37] P.L. Bishay, C. Aguilar, Parametric study of a composite skin for a twist-morphing wing, *Aerospace* 8 (2021) 259.